Annu. Rev. Phys. Chem. 1999. 50:537–70

CONSTRUCTING MULTIDIMENSIONAL MOLECULAR POTENTIAL ENERGY SURFACES FROM AB INITIO DATA

Timothy Hollebeek, Tak-San Ho, and Herschel Rabitz
Department of Chemistry, Princeton University, Princeton, New Jersey 08544-1009; e-mail: tim@wfn-shop.princeton.edu; taksan@wfn-shop.princeton.edu; hrabitz@chemvax.princeton.edu

Key Words reproducing kernel, chemical dynamics

■ **Abstract** This paper describes the reproducing kernel Hilbert space (RKHS) method for constructing accurate, smooth, and efficient global potential energy surface (PES) representations for polyatomic systems using high-level ab initio data. The RKHS method provides a rigorous and effective framework for smooth multivariate interpolation of arbitrarily scattered data points and also for incorporating various physical requirements onto the PESs. Smoothness, permutation symmetry, and the asymptotic properties of polyatomic systems can be incorporated into the construction of reproducing kernels to render globally accurate PESs. Tensor products of one-dimensional generalized-spline-reproducing kernels are amenable to a fast algorithm, which makes a single evaluation of RKHS PESs essentially independent of the number of interpolated ab initio data points. This efficient implementation enables the study of the detailed dynamics of polyatomic systems based on high-quality RKHS PESs.

INTRODUCTION

During the past two decades, there have been dramatic improvements in both the accuracy and efficiency of high-level electronic structure calculations (1–4). These advances, along with the increasing speed of modern computers, have made possible very high-quality ab initio calculations for small polyatomic systems (5, 6). For three- and four-atom systems, calculations with errors less than 1 kcal/mol are feasible. Gradients and Hessians are also becoming widely available. However, many uses of this vast supply of data require that it be reexpressed with a suitable local or global representation as a potential energy surface (PES). Since the inception of quantum mechanics, considerable effort has been devoted to finding better ways of utilizing ab initio data and/or experimental data to construct PESs. The earliest and most common methods involve least-squares fitting to empirical or

semiempirical functional forms (7–9). This approach is mature and well understood, although sophisticated schemes involving complex functional forms continue to evolve. During the past decade, generic multivariate interpolation techniques have gathered attention as alternatives to complicated functional forms (10–13). The goal of these methods is to produce a general framework for constructing PESs that will reduce the effort and expertise required to turn high-level calculations into usable surfaces. The main goal of this article is to describe one particular generic multidimensional interpolation approach, the reproducing kernel Hilbert space (RKHS) method (11–13), recently formulated for constructing accurate and efficient PES representations for small polyatomic systems to facilitate subsequent spectroscopic and dynamics studies (14–16).

Another solution is to skip the surface construction step entirely and to use the ab initio results directly in dynamical studies (17–19). However, such direct dynamics techniques are inherently classical trajectory approaches and require tens of ab initio calculations for dynamically significant trajectories, and thus, this approach is limited by the available electronic structure calculation techniques. Its application has been restricted to cases in which modest potential quality seems sufficient and in which discrete spectral lines or state-selected dynamics are not required, as in rate constant calculations based on classical trajectories (20) or in transition state theory (21, 22). In contrast, the highest-accuracy ab initio calculations can take hours or more of computer time, even for small systems. Thus, the construction of accurate analytic representations of PES is a necessary step in full quantum spectroscopic and dynamics studies that adequately model results of state-of-the-art experiments.

The number of high-level ab initio data points currently needed for adequate sampling of dynamically significant regions typically ranges from several hundred to several thousand points for tri- and tetra-atomic systems. Methods that use derivatives typically use fewer configurations; however, the number of pieces of information is typically in the same range (23–26). Consequently, with conventional surface construction methods, the number of fitting parameters and thus the complexity of the functional form needed to adequately represent the data, quickly becomes unmanageable.

Such complicated fitting forms are required because the errors in the highest level ab initio calculations are quite small. Every term in a conventional prescribed functional form must be carefully crafted so that it (*a*) does not introduce arbitrary features, (*b*) achieves the required smoothness, (*c*) preserves any necessary permutation symmetry, and (*d*) agrees with any known asymptotic form of the underlying PES. An analytic fit that has a residual significantly larger than the error in the high level ab initio calculations is only marginally more useful than if a lower-level calculation is employed. High-quality ab initio calculations demand representations that preserve their level of accuracy.

Despite the difficulty of employing prescribed forms for fitting, there are several examples of carefully crafted analytic representations: (*a*) the Liu-Siegbahn-Truhlar-Horowitz (LSTH) H_3 surface (27–30); (*b*) the many-body Sorbie-Murrell

(SM) surfaces (7, 31, 32); (*c*) the many-body expansion technique of Aguada & Paniagua (33–34); (*d*) the energy-switching (ES) approach of Varandas (35–37); (*e*) the double many-body expansion (DMBE) surface (38, 39); (*f*) the semiempirical diatomics-in-molecules (DIM) method of Kuntz (40); (*g*) the N-body explicitly correlated Gaussian-basis function method of Kinghorn & Adamowicz (41); and (*h*) the continued improvement of the Hartree-Fock-plus-dispersion (HFD) fitting methods for van der Waals potential energy surfaces (42, 43). In the past decade, intense effort in these areas has produced a host of much-improved global triatomic PESs, including (*a*) a new H_3 surface (30); (*b*) an HCP surface (31); (*c*) $H + Cl_2$ surfaces (32); (*d*) an improved $F + H_2$ surface (44); (*e*) a new Li + HF surface (34); (*f*) an H_2O surface that has spectroscopic accuracy around the equilibrium region and also correctly accounts for the long-range forces (35); (*g*) some multivalued PESs, including H_2O (36, 37) and NaHF (45); and (*h*) many improved HFD-type PESs, including HeCO (46, 47) and $ArCO_2$ (48). Notwithstanding these successes, the application of this kind of approach to construction of tetra-atomic PESs for reactive systems like $CN + H_2$ (49), $OH + H_2$ (50), and $H + O_3$ (39) has been less successful and presents a serious challenge. Once a surface has been constructed, the empirical and least-squares PES representations are usually computationally inexpensive. However, they are often not flexible enough for satisfactorily approximating accurate ab initio calculations. Moreover, they often exhibit nonphysical features that can seriously hinder theoretical studies in spectroscopy and dynamics.

Recently, Wu et al (51) obtained a very accurate global PES based on a simple three-dimensional (3-D) cubic spline interpolation method for the ground electronic state of H_3. Exact quantum Monte Carlo (EQMC) (52) calculations on a dense grid of 76,000 nuclear configurations with a statistical error of only 0.01 kcal/mol were used as input for the spline interpolation. This new PES is an order of magnitude more accurate than the best PES previously obtained for the same system. This surface allows precise calculation of scattering resonances and other features that are extremely sensitive to the shape of the PES. A simple spline is capable of accurately representing this surface because of the dense sampling and the use of a regular grid.

Attention has focused on the application of traditional multidimensional interpolation methods directly to the representation of surfaces (54), as well as on a number of new methods tailored specifically to the problem of representing PESs. Some of these new developments include (*a*) the modified Shepard (MS) method of Ischtwan & Collins (10), which uses the energy, gradient, and Hessian from ab initio data, in conjunction with trajectory calculations, to interpolate and to iteratively improve the relevant PESs (10, 23–26, 53, 55–57a); (*b*) the RKHS method that provides a rigorous and efficient framework for fast and smooth multivariate interpolation (11–14); (*c*) the product representation (PR) method of Jäckle & Meyer (58, 58a), which adopts a linear combination of products of one-dimensional (1-D) functions, the so-called natural potentials explicitly derived from gridded data points; and (*d*) the distributed approximating functional (DAF) method (59) that is based on polynomials, orthogonal under summation over a discrete set of

points with Gaussian weight functions. Unlike the PR and DAF methods, which are actually quasi-interpolation procedures (they do not recover the input ab initio data exactly), the MS and RKHS methods are true interpolation procedures that can reproduce the input data (including the potential energy values and derivatives) exactly. The PR method has been applied to the construction of a 3-D NOCl surface, a six-dimensional (6-D) model Coulomb potential, and a surface based on data constructed from the 3-D LSTH H_3 potential (58, 58a), whereas the DAF method has been used for constructing 1-, 2-, and 3-D model potentials (59). Thus far, only the MS and RKHS interpolation methods have been actively pursued to yield PESs that have been subjected to rigorous dynamics studies for comparison with recent experimental results. Both the MS and RKHS approaches are general global interpolation techniques using scattered data points in multidimensional spaces and can be readily invoked to generate interpolatory-quality PESs for any polyatomic system regardless of how the ab initio data points are distributed over the whole, or portions of, molecular configuration space. This general feature has been successfully demonstrated by both the MS and RKHS methods, particularly for their applications to both van der Waals molecules and reactive systems. The MS method, which is restricted to the use of classical trajectories, has recently been applied to the construction of PESs of some proto-typical reactive systems, including $NH + H_2$, $OH + H_2$ (23, 24), $H + H_2$ (25), $O + H_2$ (53), $CH_2OH^+ \rightarrow CHO^+ + H_2$ (57, 57a), $C + H_3^+$ (55), and $CH_3 + H_2$ (26). The main drawback of a global interpolating function is that its evaluation cost is, in general, proportional to the number of the data points contained in the interpolation. Consequently, when a large number of ab initio points are required, proper localization schemes need to be implemented. This can be done by only using a small number of neighboring data points for evaluating each PES functional point, by introducing appropriate mollifying functions that have compact support or that decay rapidly with distance, or by using a cutoff radius, as in the MS method. However, many of these localization schemes can be difficult to implement for problems other than those for 1-D, and they can introduce discontinuities at the cutoff boundaries, causing small nonphysical features that can be problematic for trajectory studies. As a special case, the RKHS method can be formulated in terms of tensor products of 1-D generalized spline-reproducing kernels to render smooth, efficient, and accurate interpolating PES representations. A single evaluation of the resulting RKHS PES function is essentially independent of the number of interpolated data points.

The RKHS method is intimately related to the reconstruction of multivariate functions from scattered data in certain linear functional spaces. It has been shown that these functional spaces must depend on the data to have a unique solution (60) and that such data-dependent spaces are closely related to positive definite functions (61). The reproducing kernel $Q(\mathbf{x}, \mathbf{x}')$ (see below) that is associated with an RKHS $\mathcal{H}(\mathcal{D})$ in the spatial domain $\mathcal{D}$, over the multidimensional coordinate $\mathbf{x}$, is unique and positive-definite, and thus constitutes a natural basis for generic multivariate interpolation problems. The RKHS theory has a history that goes

back several decades (61–64) and is closely related to the study of conformal mappings (65), integral equations (66), and partial differential equations (67). The RKHS theory provides a unified framework for stochastic processes and signal processing (64, 68). Recently, the RKHS technique has also been invoked for the formulation of generalized smooth (surface) spline functions in Sobolev spaces (69–73) [using the RKHSs based on inner products involving derivatives of continuously differentiable functions (74)]. Based on these fundamental developments, the RKHS method has been adopted for a variety of applications, especially for data interpolation and smoothing (75). Recently, the method has also been applied to accurate construction of smooth global PESs for a number of molecules, including He_2, HeCO, H_3^+ (11), Na_3 (76), $O(^1D) + H_2$ (14, 15), and $N + H_2$ (77–79; implementations of these and other PESs may be downloaded from http://wfw-shop.princeton.edu/PES), based on both scattered and regularly gridded high-level ab initio calculations. Its use in solving bound-state problems has also been investigated (80, 81). In particular, 1-D generalized spline-reproducing kernels tailored to specific smoothness, symmetry, and asymptotic behavior have been constructed (11). Using these 1-D reproducing kernels, multidimensional reproducing kernels in tensor-product forms can, in turn, be constructed to achieve highly efficient PES representations for small polyatomic systems. Moreover, the RKHS method provides a general framework for interpolating not only the energy values but also the gradients and Hessians made available in recent ab initio calculations.

The article is arranged as follows: The next section describes the general theory of the RKHS method. In the following section, the core of the RKHS method is presented, as well as the procedure for construction of the reproducing kernels, especially of 1-D types with specific smoothness and asymptotic forms that are used to build multidimensional kernels. The next section describes the fast algorithm for evaluating tensor-product RKHS PES representations. The section that follows is a description of an extension of the fast algorithm to arbitrarily shaped regions. Several representative RKHS PESs are presented after that. The final section provides an overview of the RKHS method.

REPRODUCING KERNEL HILBERT SPACE INTERPOLATION

Formally, a RKHS $\mathcal{H}(\mathcal{D})$ is a Hilbert space of continuous real-valued functions [$f(\mathbf{x})$'s] of a multivariate variable $\mathbf{x}$ defined on a multidimensional spatial domain $\mathcal{D}$. A RKHS possesses many useful properties for data interpolation and function-approximation problems. Of particular importance among them are the following (61–64). 1. Reproducing property: There exists a kernel function $Q(\mathbf{x}, \mathbf{x}')$, the reproducing kernel, in $\mathcal{H}(\mathcal{D})$ such that the following properties

$$f(\mathbf{x}) = \langle f(\mathbf{x}'), Q(\mathbf{x}, \mathbf{x}') \rangle' \qquad 1.$$

and

$$Q(\mathbf{x}, \mathbf{y}) = \langle Q(\mathbf{x}, \mathbf{x}'), Q(\mathbf{y}, \mathbf{x}')\rangle' \tag{2.}$$

hold. The prime $'$ indicates that the inner product $\langle,\rangle'$ is performed over $\mathbf{x}'$; 2. Uniqueness: The RKHS $\mathcal{H}(\mathcal{D})$ has one, and only one, reproducing kernel $Q(\mathbf{x}, \mathbf{x}')$; and 3. Symmetry and Positivity: The reproducing kernel $Q(\mathbf{x}, \mathbf{x}')$ is symmetric,

$$Q(\mathbf{x}, \mathbf{x}') = Q(\mathbf{x}', \mathbf{x}), \tag{3.}$$

and positive-definite,

$$\sum_{i=1}^{n}\sum_{j=1}^{n} c_i\, Q(\mathbf{x}_i, \mathbf{x}_j) c_j \geq 0, \tag{4.}$$

for any set of real numbers c_i and for any countable set of points $\mathbf{x}_i$, $i = 1, \ldots, n$.

Interpolation as an Inverse Problem

Within the general framework of the RKHS method, an interpolation problem in a multidimensional spatial domain $\mathcal{D}$, like the molecular configuration space of N-atoms defined via a set of $D = 3N - 6$ independent internal coordinates, can be posed as follows: Given a set of real-valued data $\{f_i\}_{i=1}^{M}$ specified at M distinct points $\mathcal{S}_M = \{\mathbf{x}_i,\ i = 1, \ldots, M\}$ in a D-dimensional domain $\mathcal{D}$, and a RKHS $\mathcal{H}(\mathcal{D})$, find a suitable function $f(\mathbf{x})$ that interpolates these data points. Explicitly, when using the reproducing property (Equation 1), the above interpolation problem is reduced to solving the following linear inverse problem (82):

$$f(\mathbf{x}_i) = \langle f(\mathbf{x}'), Q(\mathbf{x}_i, \mathbf{x}')\rangle' \quad i = 1, \ldots, M, \tag{5.}$$

where the goal is to invert this relation to find the function $f(\mathbf{x})$ in $\mathcal{H}(\mathcal{D})$. The linear inverse problem posed in Equation 5 is a generalized Fredholm-integral equation of the first kind with discrete data, and there exist a host of powerful techniques for solving this problem. In the context of the present work, $f(\mathbf{x}_i)$, $i = 1, 2, \ldots$ on the left-hand side is the ab initio data at configuration space points x_i, and $f(\mathbf{x}')$ on the right-hand side is the desired PES to be extracted by solving this equation. The following discussion presents the normal solution that renders true interpolation of the input data points and the regularized solution that yields quasi-interpolatory results, accompanied by an error bound analysis. The construction of an appropriate RKHS to solve the problem is discussed in the next section. The choice of RKHS encapsulates all the known information about required symmetry properties, asymptotic form, and smoothness constraints.

Normal Solutions

The most straightforward approach is to find the normal solution for the PES $f^{\dagger}(\mathbf{x})$ that has the minimal squared norm (11),

$$\| f^{\dagger} \|^2 = \langle f^{\dagger}(\mathbf{x}'),\ f^{\dagger}(\mathbf{x}') \rangle', \tag{6.}$$

subject to the interpolation condition (Equation 5). It is easy to show that the normal solution $f^{\dagger}(\mathbf{x})$ of Equation 5 is

$$f^{\dagger}(\mathbf{x}) = \sum_{i=1}^{M} c_i\, Q(\mathbf{x}_i, \mathbf{x}), \tag{7.}$$

where the coefficients c_i satisfy the linear relation

$$\sum_{i=1}^{M} c_i\, Q_{ij} = f_j, \quad j = 1, \ldots, M, \tag{8.}$$

with $Q_{ij} = Q(\mathbf{x}_i, \mathbf{x}_j)$. In order for this to be useful, the symmetric positive-definite (Equation 4) $M \times M$ matrix $\mathbf{Q}_M \equiv [Q_{ij}]$ must be well-conditioned. If it is, then the linear algebraic equation Equation 8 can be efficiently solved by using the Cholesky decomposition method (83). Otherwise, use of more sophisticated techniques may be necessary.

Regularized Solutions

When the matrix $\mathbf{Q}_M$ becomes ill conditioned, because of either a large number of data points or clusters of data points, effective and numerically stable regularization procedures may be invoked for approximately solving the linear inverse problem in Equation 5. In particular, the Tikhonov regularization procedure (84) produces an approximate solution, $f_{\alpha}^{\dagger}(\mathbf{x})$, which belongs to the space $\mathcal{H}(\mathcal{D})$, which can be obtained via the minimization of the regularization functional

$$J[\tilde{f}; \alpha] = \| \mathbf{Q}\tilde{f} - \mathbf{f} \|^2 + \alpha \| \tilde{f} \|^2, \tag{9.}$$

with respect to the function $\tilde{f}(\mathbf{x})$. Here, the residual norm $\| \mathbf{Q}\tilde{f} - \mathbf{f} \|^2$ is defined as

$$\| \mathbf{Q}\tilde{f} - \mathbf{f} \|^2 = \sum_{i=1}^{M} \{ \langle \tilde{f}(\mathbf{x}'),\, Q(\mathbf{x}_i, \mathbf{x}') \rangle' - f_i \}^2; \tag{10.}$$

the input ab initio data vector is $\mathbf{f} = \{ f_1, \ldots, f_M \}$, and the function magnitude constraint $\| \tilde{f} \|^2$ is defined via Equation 6. The regularization parameter $\alpha > 0$ is chosen to impose a proper balance between the residual constraint $\| \mathbf{Q}\tilde{f} - \mathbf{f} \|$ and the magnitude constraint $\| \tilde{f} \|$. The norm term $\| \tilde{f} \|$ acts as a regularizer for the calculation by aiming to eliminate nonphysical oscillations in the PES. The regularized solution $f_{\alpha}^{\dagger}(\mathbf{x})$, which minimizes the functional $J[\tilde{f}; \alpha]$, has the form

$$f_{\alpha}^{\dagger}(\mathbf{x}) = \sum_{i=1}^{M} c_i^{\alpha}\, Q(\mathbf{x}_i, \mathbf{x}), \tag{11.}$$

where the coefficients c_i^α satisfy the linear relation

$$\sum_{i=1}^{M} c_i^\alpha \{Q_{ij} + \alpha\delta_{ij}\} = f_j, \quad j = 1, \ldots, M, \tag{12.}$$

with δ_{ij} being the Kronecker delta function. For $\alpha > 0$, the matrix $\mathbf{Q}_M^\alpha = \{Q_{ij} + \alpha\delta_{ij}\}$ is symmetric and positive-definite, thus the Cholesky decomposition method can again be used to facilitate the solution to Equation 12. At the core of the regularization procedure is an adequate algorithm for determining the value of the regularization parameter α to render a meaningful solution that is continuous with respect to an arbitrary small change in the values of the data $\{f_i\}$ that produces a good recovery of the input data $\{f_i\}$ at the discrete points $\{\mathbf{x}_i\}$, and that is smooth (does not contain any spurious oscillatory features between data points). There exist a variety of effective procedures for determining the value of α. For data $f_i, i = 1, 2, \ldots$ that are very accurate (for example, from high-level ab initio calculations) or of a nonstatistical nature, the value of α can, in general, be simply calculated from the product $\epsilon_m\omega_1^2$, with ϵ_m being the unit machine roundoff, and with ω_1^2 the largest of the singular values $\omega_1^2 > \cdots > \omega_M^2 > 0$ of the symmetric matrix $\mathbf{Q_M}$ (cf, Equation 8) (11, 83). On the other hand, for data that are characterized by statistical errors [for example, from first principle Monte Carlo calculations (52)], the value of α can be determined by invoking the straightforward discrepancy principle (82) that conforms to the given data error bound or the more sophisticated generalized cross-validation (GCV) method (75) that measures the averaged prediction errors of an arbitrary data point that is left out.

A Posteriori Error Bound

A fundamentally important feature of the RKHS interpolation method is that it leads to an automatic error estimate of the regularized solution $f_\alpha^\dagger(\mathbf{x})$ in Equation 11. The normal PES solution $f^\dagger(\mathbf{x})$ is the special case of $f_\alpha^\dagger(\mathbf{x})$ with $\alpha = 0$. In general, there are two sources of errors pertinent to the regularized PES solution $f_\alpha^\dagger(\mathbf{x})$: (*a*) the use of only a finite number of ab initio data points $f_i, i = 1, \ldots, M$, and (*b*) the adoption of the regularization procedure. Although a large number of (distinct) data points can lead to a converged PES, they inevitably render the corresponding linear inverse problem unstable (Equation 5). For a given set of data points, an a posteriori error bound can be readily assigned to the regularized solution $f_\alpha^\dagger(\mathbf{x})$, with use of the reproducing properties (Equation 1) and (Equation 2) and the Schwartz inequality (62).

Let the function $f(\mathbf{x})$ be the true PES solution of the linear inverse problem (Equation 5). First, the absolute deviation $|f(\mathbf{x}) - f_\alpha^\dagger(\mathbf{x})|$ can be written as

$$|f(\mathbf{x}) - f_\alpha^\dagger(\mathbf{x})| = |\langle f(\mathbf{x}'), \Delta_{\mathbf{x}}(\alpha; \mathbf{x}')\rangle'|, \tag{13.}$$

where the difference function $\Delta_{\mathbf{x}}(\alpha; \mathbf{x}')$ is defined as

$$\Delta_{\mathbf{x}}(\alpha; \mathbf{x}') = Q(\mathbf{x}, \mathbf{x}') - \sum_{i=1}^{M} Q_i^{\dagger}(\alpha, \mathbf{x}) Q(\mathbf{x}_i, \mathbf{x}'). \tag{14.}$$

The regularized cardinal function $Q_i^{\dagger}(\alpha, \mathbf{x})$ is defined as

$$Q_i^{\dagger}(\alpha, \mathbf{x}) = \sum_{j=1}^{M} \left[\mathbf{Q}_M^{\alpha}\right]_{ij}^{-1} Q(\mathbf{x}_j, \mathbf{x}), \tag{15.}$$

with $[\mathbf{Q}_M^{\alpha}]^{-1}$ being the inverse of the matrix $\mathbf{Q}_M^{\alpha}$ (cf, Equation 12). In deriving Equation 14, we have used the reproducing properties in Equations 1 and 2.

By invoking the Schwartz inequality (62)

$$|\langle f(\mathbf{x}'), g(\mathbf{x}')\rangle'| \leq \|f\| \, \|g\|, \tag{16.}$$

for any two functions $f(\mathbf{x})$ and $g(\mathbf{x})$ belonging to the RKHS $\mathcal{H}(\mathcal{D})$, one can derive the relation

$$|f(\mathbf{x}) - f_{\alpha}^{\dagger}(\mathbf{x})| \leq \|f\| \, \|\Delta_{\mathbf{x}}(\alpha)\|, \tag{17.}$$

where the square of the relative error bound $\|\Delta_{\mathbf{x}}(\alpha)\|$ at the position $\mathbf{x}$, and as a function of α, takes on the simple form

$$\|\Delta_{\mathbf{x}}(\alpha)\|^2 = Q(\mathbf{x}, \mathbf{x}) - 2\sum_{i=1}^{M} Q_i^{\dagger}(\alpha, \mathbf{x}) Q(\mathbf{x}_i, \mathbf{x}) + \sum_{i=1}^{M}\sum_{j=1}^{M} \mathbf{Q}_{ij} Q_i^{\dagger}(\alpha, \mathbf{x}) Q_j^{\dagger}(\alpha, \mathbf{x}). \tag{18.}$$

It is readily seen that if the matrix $\mathbf{Q}_M$ is assumed to be nonsingular, then $Q_i^{\dagger}(\alpha, \mathbf{x}_j)$ equals δ_{ij} in the limit of $\alpha = 0$, and the regularized cardinal function $Q_i^{\dagger}(\alpha, \mathbf{x})$ becomes a true cardinal function. Therefore, Equation 18 becomes

$$\|\Delta_{\mathbf{x}}(\alpha = 0)\|^2 = Q(\mathbf{x}, \mathbf{x}) - \sum_{i=1}^{M}\sum_{j=1}^{M} [\mathbf{Q}_M]_{ij}^{-1} Q(\mathbf{x}_i, \mathbf{x}) Q(\mathbf{x}_j, \mathbf{x}), \tag{19.}$$

which vanishes at each data point $\mathbf{x} = \mathbf{x}_i, i = 1, \ldots, M$, in accordance with the fact that the normal solution $f^{\dagger}(\mathbf{x})$ in Equation 7 is interpolatory.

Equation 17 shows that the bound on the error consists of two parts: $\|f\|$ is an unknown constant, and the $\mathbf{x}$ dependence of the error is entirely contained in the $\|\Delta_{\mathbf{x}}(\alpha)\|$ term. This second term depends only on the kernel and distribution of the data points and is independent of the f_i values. It measures the relative uncertainty due to the finite number of data points used in the interpolation and is helpful in determining the arrangement of data points that will give the best representation of an arbitrary function. It also allows the evaluation of different RKHSs in order to find the one most appropriate for a given problem.

If the values $f_i, i = 1, 2, \ldots$ are representative of the behavior of the true PES function $f(x)$, then $\| f_\alpha^\dagger \|$ is a reasonable approximation for $\| f \|$, and the a posteriori absolute bound

$$\epsilon_\alpha(\mathbf{x}) = \| \Delta_\mathbf{x}(\alpha) \| \, \| f_\alpha^\dagger \| \qquad 20.$$

gives a quantitative estimate of an upper bound for the error as a function of $\mathbf{x}$.

In the $\alpha = 0$ case, $\| f^\dagger \|^2 = \sum_{i=1}^M \sum_{j=1}^M c_i c_j Q_{ij} = \sum_{i=1}^M c_i f_i$ (Equations 6, 7, 8). This result shows that the coefficients give the sensitivity of the norm to each particular ab initio data point and thus indicate which areas of the surface contribute the most to the overall norm. These sensitivities, along with the relative error bound $\| \Delta_\mathbf{x}(\alpha) \|$, can be used to determine where additional ab initio calculations would be most helpful.

CONSTRUCTION OF REPRODUCING KERNELS

In this section, we describe several examples that are useful for constructing global PES representations for polyatomic systems with use of high-level ab initio electronic structure calculations. The molecular coordinates of interest are D-independent internal coordinates $\mathbf{x} = \{x_1, \ldots, x_D\}$ that define a molecular configuration space $\mathcal{D}$. These internal coordinates are typically bond distances, bond angles, or various other coordinates that belong either to the semi-infinite interval $[0, \infty)$ or to a finite interval like $[0, 1]$ or $[0, 2\pi]$. In addition to the coordinate system, other PES attributes, including smoothness, symmetry, and asymptotic behavior, can also play a role in the construction of the kernels. Although generic kernels perform adequately, additional accuracy can be attained through careful attention to the kernels used in the representation. In most circumstances, it is difficult to construct genuine multivariate reproducing kernels with the necessary physical properties required to adequately represent a multidimensional PES for an arbitrary polyatomic system. Multidimensional kernels are most accessible in terms of Cartesian coordinates, and as a result, smooth kernels of dimensions ≥ 2 in general are radial-basis functions that only depend on the usual Euclidean norm (the distance between two distinct positions) (60, 72, 73). However, for molecular PES representations, the construction of multidimensional reproducing kernels as a simple tensor product of 1-D kernels has many advantages because it allows the appropriate features of each dimension to be included independently.

A D-dimensional RKHS $\mathcal{H}(\mathcal{D})$ in tensor-product form can be readily written as a direct product (11)

$$\mathcal{H}(\mathcal{D}) = \mathcal{H}_1 \otimes \cdots \otimes \mathcal{H}_D, \qquad 21.$$

in terms of 1-D RKHSs $\mathcal{H}_1, \ldots, \mathcal{H}_D$ corresponding to D-independent internal coordinates $x_1, \ldots, x_D$. Likewise, the associated D-dimensional reproducing kernel

$Q(\mathbf{x}, \mathbf{x}')$ can be expanded into the product form

$$Q(\mathbf{x}, \mathbf{x}') = \prod_{i=1}^{D} q_i(x_i, x_i'), \qquad 22.$$

where the 1-D reproducing kernel $q_i(x_i, x_i')$ is associated with the RKHS $\mathcal{H}_i$ and possesses the reproducing property

$$f(x_i) = \langle f(x_i'), q(x_i, x_i') \rangle_i' \qquad 23.$$

for every function $f(x_i)$ belonging to $\mathcal{H}_i$. The subscript i that appears in $\langle , \rangle_i'$ denotes that the inner product is taken over the ith internal coordinate x_i.

To build multidimensional kernels that are appropriate to a wide variety of problems, we need a collection of 1-D reproducing kernels that can appropriately represent any situation that might be encountered, by allowing the smoothness and asymptotic form to be specifically tailored to the problem at hand. Any required permutation symmetry of the PES can be easily included by further symmetrization of the product form in Equation 22.

It is known that (generalized) smooth spline functions, including polynomial splines, are intimately related to reproducing kernels of appropriate Hilbert spaces, endowed with inner products involving derivatives, and possess many important minimum properties following from orthogonal projections in Hilbert spaces (69). A relationship for constructing smooth reproducing kernels is Taylor's formula with integral remainder (62)

$$f(x) = \sum_{k=0}^{n-1} \frac{f^k(y)(x-y)^k}{(k)!} + \frac{1}{(n-1)!} \int_y^x (x-x')^{n-1} f^{(n)}(x')\, dx', \qquad 24.$$

where the variables x and y belong to the interval $[a, b]$, $-\infty < a < b < \infty$, and the derivatives are $f^{(k)}(x) = \frac{d^k f(x)}{dx^k}$, $k = 0, \ldots, n$. Taylor's formula embodies the reproducing property, as shown in Equation 23, that arises from a RKHS endowed with a particular inner product that involves derivatives of the constituent functions. Another useful tool, which is a direct result of Taylor's formula, is Peano's general remainder formula (62, 69),

$$\hat{\mathbf{L}}[f] = \frac{1}{(n-1)!} \int_a^b f^{(n)}(x')\, \hat{\mathbf{L}}_x[(x-x')_+^{n-1}]\, dx', \qquad 25.$$

where $\hat{\mathbf{L}}$ is an arbitrary linear functional, such that $\hat{\mathbf{L}}[p] = 0$ for all polynomials $p(x)$ of an order less than or equal to $n-1$. The notation $\hat{\mathbf{L}}_x[(x-x')_+^{n-1}]$ indicates that the functional $\hat{\mathbf{L}}_x$ is applied to $(x-x')_+^{n-1}$, considered as a function of x, and that

$$(x-y)_+^k = \begin{cases} (x-y)^k, & \text{if } x \geq y; \\ 0, & \text{if } x < y. \end{cases} \qquad 26.$$

Both Taylor's and Peano's formulae can be used to construct smooth reproducing kernels that are characterized by a small integer n, which indicates the order

of smoothness of the resulting kernel. In the following, we give some examples of smooth 1-D reproducing kernels based on Taylor's and Peano's formulas. The first three come from direct use of Taylor's formula, and the final two are the results of using Peano's formula. The first example describes in some detail the three steps that lead to the desired smooth reproducing kernel: (*a*) start with the definition of an inner product that involves derivatives and a proper weight function, (*b*) derive an integral representation for the reproducing kernel by explicit use of the remainder formula and the reproducing property that arises from the RKHS method theory, and (*c*) arrive at a simple closed-form expression by carrying out the integral in step 2 and by comparing with the reproducing property in Equation 23. The same basic steps are used to construct the remaining four kernels.

Reciprocal Power Reproducing Kernels over the Interval $[0, \infty)$

In the first example, we consider reciprocal power (RP) reproducing kernels that asymptotically behave as some RP of the distance variable x over the interval $[0, \infty)$. Without loss of generality, we shall assume that the function $f(x)$ of interest possesses the asymptotic property

$$\lim_{x\to\infty} x^k f^{(k)}(x) = 0, \quad k = 1, \ldots, n-1. \tag{27.}$$

We note that apart from a constant energy shift, the leading term of a molecular PES at large separations is usually proportional to some RP of the appropriate distance variable x. Hence, this particular kernel is useful for treating the degrees of freedom that describe the approach of two molecular fragments in a van der Waals or reactive system.

Following the first step, a smooth reproducing kernel $q^{\mathrm{RP}}(x, x')$ can be constructed via a proper definition of the inner product, between any two functions $f(x)$ and $g(x)$. Here, the choice is (11)

$$\langle f(x'), g(x')\rangle' = \int_0^\infty \frac{x'^n f^{(n)}(x')}{n!} \frac{x'^n g^{(n)}(x')}{n!} \frac{dx'}{w(x')}, \tag{28.}$$

where $w(x') = x'^{-m}$, $m \geq 0$ is the correct asymptotic weighting function for this case. From the reproducing property (Equation 23) and the explicit use of the inner product (Equation 28), we have

$$f(x) = \langle f(x'), q^{\mathrm{RP}}(x, x')\rangle' = \int_0^\infty \frac{x'^n f^{(n)}(x')}{n!} \frac{x'^n \partial^n q^{\mathrm{RP}}(x, x')/\partial x'^n}{n!} \frac{dx'}{w(x')}. \tag{29.}$$

Then, in the second step, by comparing Equation 29 with Taylor's formula (Equation 24), with a choice of the reference point $y = \infty$ and the use of the

asymptotic property (Equation 27), one can readily derive the relation

$$\frac{x'^n}{n!}\frac{\partial^n q^{\mathrm{RP}}(x,x')}{\partial x'^n} = n(x'-x)_+^{n-1}x'^{-n}w(x') \qquad 30.$$

and, therefore, the corresponding reproducing kernel of the integral representation

$$\begin{aligned} q^{\mathrm{RP}}(x,x') &= \langle q^{\mathrm{RP}}(x,x''), q^{\mathrm{RP}}(x',x'')\rangle'' \\ &= n^2\int_0^\infty (x''-x)_+^{n-1}(x''-x')_+^{n-1}x''^{-(2n+m)}\,dx'', \end{aligned} \qquad 31.$$

taking into account the explicit reciprocal power weight $w(x'') = x''^{-m}$.

In the final step, the integral in Equation 31 is carried out and we obtain the RP reproducing kernel in the closed form,

$$q^{\mathrm{RP}}_{n,m}(x,x') = n^2\,x_>^{-(m+1)}\,\mathrm{B}(m+1,n)\,{}_2\mathrm{F}_1\left(-n+1, m+1; n+m+1; \frac{x_<}{x_>}\right), \qquad 32.$$

where $x_>$ and $x_<$ are, respectively, the larger and smaller of x and x'; $\mathrm{B}(a,b)$ is the beta function; and ${}_2\mathrm{F}_1(a,b;c;z)$ is the Gauss' hypergeometric function. The integers $n-1$ and $m+1$ designate, respectively, the order of smoothness and the asymptotic RP behavior of the reproducing kernel $q^{\mathrm{RP}}(x,x')$. This kernel is a rational polynomial in the variables x and x' and has only a finite number of terms, so it is computationally efficient and compact. This property is also important to the fast algorithm (see below).

Exponential Decaying Reproducing Kernels over the Interval $[0,\infty)$

In the second example, we consider exponential decaying (ED) reproducing kernels that decrease exponentially to zero at large distances x. Short-range contributions to intermolecular interactions often have this sort of scaling. A smooth ED reproducing kernel $q^{\mathrm{ED}}(x,x')$ may be constructed via the following definition of the inner product,

$$\langle f(x'), g(x')\rangle' = \int_0^\infty \frac{f^n(x')}{n!}\frac{g^{(n)}(x')}{n!}e^{\beta x'}dx', \qquad 33.$$

with the real-valued constant $\beta > 0$. Following similar steps taken in obtaining the RP reproducing kernel, we can readily derive the integral representation for the ED reproducing kernel,

$$q^{\mathrm{ED}}(x,x') = n^2\int_0^\infty (x''-x)_+^{n-1}(x''-x)_+^{n-1}e^{-\beta x''}dx'', \qquad 34.$$

which can be easily carried out to yield the closed form

$$q_n^{\mathrm{ED}}(x, x') = \frac{n\, n!}{\beta^{2n-1}} e^{-\beta x_>} \sum_{k=0}^{n-1} \frac{(2n-2-k)!}{(n-1-k)!k!} [\beta(x_> - x_<)]^k, \quad \beta > 0. \qquad 35.$$

Taylor Spline Reproducing Kernels over the Interval [0, 1]

In the third example, we construct Taylor spline (TS) reproducing kernels over the interval [0, 1]. Appropriate scaling and translation allow this kernel to handle any finite interval, such as the range of an angular coordinate in a typical PES coordinate system. For simplicity, we consider $x = 0$ as the reference point (other reference points are possible) in Taylor's formula (Equation 24) and introduce the inner product (11, 82)

$$\langle f(x'), g(x') \rangle' = \sum_{k=0}^{n-1} \frac{f^{(k)}(0)}{k!} \frac{g^{(k)}(0)}{k!} + \int_0^1 \frac{f^{(n)}(x')}{n!} \frac{g^{(n)}(x')}{n!} \frac{dx'}{w(x')}. \qquad 36.$$

As before, the use of the reproducing property (Equation 23) and a comparison with Taylor's formula (Equation 24) gives the TS reproducing kernel $q^{\mathrm{TS}}(x, x')$:

$$q^{\mathrm{TS}}(x, x') = \sum_{i=0}^{n-1} x^i x'^i + n^2 \int_0^1 (x-y)_+^{n-1} (x'-y)_+^{n-1} w(y)\, dy. \qquad 37.$$

For the special case $w(y) = 1$, it takes the closed form

$$q_n^{\mathrm{TS}}(x, x') = \sum_{i=0}^{n-1} x^i x'^i + \xi_n^{\mathrm{T}}(x, x'), \qquad 38.$$

where Taylor's remainder kernel $\xi_n^{\mathrm{T}}(x, x')$ is defined as

$$\begin{aligned} \xi_n^{\mathrm{T}}(x, x') &= n^2 \int_0^1 (x-y)_+^{n-1} (x'-y)_+^{n-1}\, dy \\ &= n x_<^n x_>^{n-1}\, {}_2F_1\left(1, -n+1; n+1; \frac{x_<}{x_>}\right). \end{aligned} \qquad 39.$$

It is a polynomial of order $2n-1$ in $x_<$ and $n-1$ in $x_>$.

The first three examples demonstrate the utility of the Taylor's formula for systematic construction of smooth reproducing kernels. The last two examples use Peano's remainder formula and illustrate how to construct smooth reproducing kernels based on Bernoulli polynomials (85) that possess strong symmetry and periodic properties, and how to construct reproducing kernels based on typical real orthonormal polynomials (86) on which rests much practical numerical analysis, including interpolation, approximation, and quadratures.

Bernoulli Polynomial Reproducing Kernels over the Interval [0, 1]

In order to construct Bernoulli polynomial (BP) reproducing kernels $q^{\mathrm{BP}}(x, x')$ defined over the interval [0, 1], we consider the inner product (75)

$$\langle f(x'), g(x')\rangle' = \sum_{k=0}^{n-1} \hat{\mathbf{I}}_{x'}^{k}[f(x')]\hat{\mathbf{I}}_{x'}^{k}[g(x')] + \int_0^1 \frac{f^{(n)}(x')}{n!}\frac{g^{(n)}(x')}{n!}\,dx', \qquad 40.$$

where the linear functional $\hat{\mathbf{I}}_{x}^{k}[f(x)]$ is defined as

$$\hat{\mathbf{I}}_{x}^{k}[f(x)] = \int_0^1 f^{(k)}(x)\,dx. \qquad 41.$$

Using the reproducing property (Equation 23), the inner product (Equation 40), and some well-known properties of the BPs, one can immediately identify the relation

$$\hat{\mathbf{I}}_{x'}^{k}[q^{\mathrm{BP}}(x, x')] = B_k(x), \qquad 42.$$

where $B_k(x)$ is the BP of the kth order. Furthermore, by invoking Peano's remainder formula (Equation 25), one can also easily derive the relation

$$\frac{\partial^n q^{\mathrm{BP}}(x, x')}{n!\,\partial x'^n} = n\left\{(x - x')_+^{n-1} - \sum_{k=0}^{n-1} B_k(x)\hat{\mathbf{I}}_{y}^{k}[(y - x')_+^{n-1}]\right\}. \qquad 43.$$

From Equations 26 and 41, we obtain

$$\hat{\mathbf{I}}_{y}^{k}[(y - x')_+^{n-1}] = \frac{(n-1)!}{(n-k)!}(1 - x')^{n-k}. \qquad 44.$$

Then, proceeding with the same steps, we derive the closed form for the reproducing kernels $q^{\mathrm{BP}}(x, x')$

$$q_n^{\mathrm{BP}}(x, x') = \sum_{k=0}^{n-1} B_k(x)B_k(x') + \xi_n^{\mathrm{BP}}(x, x'), \qquad 45.$$

where the BP remainder kernel $\xi_n^{\mathrm{BP}}(x, x')$ is defined as

$$\begin{aligned}\xi_n^{\mathrm{BP}}(x, x') = &-\sum_{k=0}^{n-1}\{B_k(x)A_{nk}(x') + A_{nk}(x)B_k(x')\} \\ &+ \sum_{k=0}^{n-1}\sum_{k'=0}^{n-1} C_{nkk'}B_k(x)B_{k'}(x') + \xi_n^{\mathrm{T}}(x, x'), \qquad 46.\end{aligned}$$

with $A_{nk}(x) = \frac{n!}{(n-k)!} x^x {}_2F_1(1, -n+k; n+1; x)$, $C_{nkk'} = \frac{(n!)^2}{(n-k)!(n-k')!(2n-k-k'+1)}$, and $\xi_n^{\mathrm{T}}(x, x')$ designated the Taylor's remainder kernel given in Equation 39. Here, the functional of the BP remainder $\hat{\mathbf{I}}_x^k[\xi_n^{\mathrm{BP}}(x, x')] = 0$ for all $k = 0, \ldots, n-1$ and leads to the periodic relations

$$\left.\frac{\partial^k \xi_n^{\mathrm{BP}}(x, x')}{\partial x^k}\right|_{x=0} = \left.\frac{\partial^k \xi_n^{\mathrm{BP}}(x, x')}{\partial x^k}\right|_{x=1},$$

which allows interpolation on intervals such as $[0, 2\pi]$ when it is important to preserve the periodic nature of the function. In particular, the Bernoulli kernel is very useful for torsion angles that often occur as coordinates in tetra-atomic and larger systems.

Orthonormal Polynomial Reproducing Kernels over the Interval [0, 1]

To construct orthonormal polynomial (OP) reproducing kernels $q^{\mathrm{OP}}(x, x')$ in the finite interval [0, 1], we define the relevant inner product as

$$\langle f(x'), g(x') \rangle' = \sum_{k=0}^{n-1} f_k g_k + \int_0^1 \frac{f^{(n)}(x')}{n!} \frac{g^{(n)}(x')}{n!}\, dx', \tag{47.}$$

where f_k and g_k are, respectively, projections of the functions $f(x)$ and $g(x)$ onto a subspace π_{n-1} spanned by OP $p_0^*(x), \ldots p_{n-1}^*(x)$, e.g. the normalized shifted Legendre polynomials, of an order equal to or less than $n-1$,

$$f_k = \int_0^1 f(x) p_k^*(x)\, dx; \quad g_k = \int_0^1 g(x) p_k^*(x)\, dx. \tag{48.}$$

When we invoke the orthonormal relations

$$\int_0^1 p_k^*(x) p_{k'}^*(x)\, dx = \delta_{kk'}, \tag{49.}$$

we can readily identify the relation

$$q_k^{\mathrm{OP}}(x) = \int_0^1 q^{\mathrm{OP}}(x, x') p_k^*(x')\, dx' = p_k^*(x). \tag{50.}$$

Again, using Peano's remainder formula, we obtain the relation

$$\frac{\partial^n q^{\mathrm{OP}}(x, x')}{n!\, \partial x'^n} = n\left\{ (x - x')_+^{n-1} - \sum_{k=0}^{n-1} p_k^*(x) s_k(x') \right\}, \tag{51.}$$

where the integral

$$s_{n,k}(x') = \int_{x'}^1 (y - x')^{n-1} p_k^*(y)\, dy \tag{52.}$$

can be easily carried out once the $(k-1)$th order polynomial $p_k^*(x)$ is specified. Consequently, the OP reproducing kernel $q^{\mathrm{OP}}(x, x')$ can be constructed to take on the expression

$$q^{\mathrm{OP}}(x, x') = K_{n-1}(x, x') + \xi_n^{\mathrm{OP}}(x, x'), \tag{53.}$$

where the well-known kernel polynomial $K_{n-1}(x, x')$ is defined as (72)

$$K_{n-1}(x, x') = \sum_{k=0}^{n-1} p_k^*(x)\, p_k^*(x') \tag{54.}$$

and the OP remainder kernel $\xi_n^{\mathrm{OP}}(x, x')$ is given by

$$\begin{aligned}\xi_n^{\mathrm{OP}}(x, x') = &- \int_0^1 K_{n-1}(x, y)\xi_n^{\mathrm{T}}(x', y)\, dy - \int_0^1 K_{n-1}(x', y)\xi_n^{\mathrm{T}}(x, y)\, dy \\ &+ \int_0^1 \int_0^1 K_{n-1}(x, y) K_{n-1}(x', y')\xi_n^{\mathrm{T}}(y, y')\, dy\, dy' + \xi_n^{\mathrm{T}}(x, x'),\end{aligned} \tag{55.}$$

with $\xi_n^{\mathrm{T}}(x, x')$ again designated as the Taylor's remainder kernel defined in Equation 39. The integrals involved in the kernel $\xi_n^{\mathrm{OP}}(x, x')$ can be readily carried out in closed form for polynomials such as the shifted Legendre polynomials.

Other kernels are possible, but these examples are appropriate for the kinds of coordinates that commonly occur in the construction of PESs. The RP kernels describe long-range interactions of fragments, whereas the ED kernels are appropriate for short-range interactions. Internal bond angles and torsion angles can be handled with TS and BP kernels, respectively. The construction of most PESs will not require the derivation of any new kernels other than those presented here.

All five reproducing kernels presented here are globally smooth functions characterized by a smoothness integer parameter n, which is usually a small number, e.g. $n = 2, 3, \ldots$. The first two reproducing kernels (the RP and ED) have been tailored to a specific asymptotic form over the interval $[0, \infty)$ and may be used to mimic the behaviors of the PES at large or small interatomic or intermolecular separations. The TS, BP, and OP reproducing kernels, over a finite interval [0, 1], are variations of polynomial spline functions, and each contains two mutually orthogonal components: a leading expansion term $\sum_{k=0}^{n-1} p_k(x)\, p_k(x')$, with specific polynomials $p_k(x)$ in each case to account for the overall form of the intended function $f(x)$ or distribution of data points over the interval, and a remainder term $\xi_n(x, x')$ to complement the behavior of the leading term. This combines the underlying behavior of a functional form with mathematically rigorous additional degrees of freedom to provide the flexibility to deal with data that cannot

be handled by the leading term. The adoption of the tensor-product construct in Equation 22 for the D-dimensional reproducing kernel $Q(\mathbf{x}, \mathbf{x}')$ in terms of 1-D smooth reproducing kernels from this section can significantly facilitate the efficient evaluation of the ab initio-RKHS PESs, cf Equation 7 or Equation 11, and thus enable realistic studies of various important molecular processes. One of the most importent advantages of multidimensional kernels of this form is explained in the following section.

A FAST ALGORITHM FOR TENSOR-PRODUCT REPRESENTATIONS

As outlined above the RKHS representation of PESs does not require that the ab initio data points form a multidimensional grid, nor does it require that the reproducing kernel be a tensor product. However, formulating a problem in those terms has important efficiency benefits (12). This requirement will be relaxed somewhat in the next section, where its application to arbitrarily shaped regions is discussed.

All of the kernels introduced above are of the general form

$$q(x, x') = \sum_{k=1}^{M_1} p_{1k}\, f_{1k}(x)\, f_{1k}(x') + \sum_{k=1}^{M_2} p_{2k}\, f_{2k}(x_<)\, f_{3k}(x_>); \qquad 56.$$

that is, they consist of sums of products of independent functions of x, x', $x_<$, and $x_>$. Representations of the PESs involve sums over terms in which one variable in the evaluations of $q(x, x')$ depends on the point being evaluated, and the other variable is fixed at a particular value.

This latter point is important because the performance bottleneck in the evaluation RKHS representations (as well as in many other types of representations) is the need to sum over as many terms as there are ab initio data points. For surfaces based on small numbers of points, this is not a problem. But in high-accuracy studies, in which one would like to use a large number of data points, it does become an issue.

In each individual term in the reproducing kernel, one half depends only on the location of a particular ab initio data point, and the other half depends only on the location where the potential is being evaluated (see Equation 56). Within each box bounded by the grid planes of the multidimensional grid that specify where the ab initio calculations are found, the dependence on the location where the potential being evaluated is can be factored out of each term. The other term is constant, regardless of where within the box the evaluation is done, and it involves the sum over all the ab initio data points. Once the constant term has been computed, it can be reused for every other evaluation within that box.

For example, in one dimension, substitution of Equation 56 into Equation 7 and reversal of the order of summation gives

$$V^{\dagger}(x) = \sum_{k=1}^{M_1} p_{1k}\, f_{1k}(x) \left(\sum_{\text{all } x_i} c_i\, f_{1k}(x_i) \right) + \sum_{k=1}^{M_2} p_{2k}\, f_{2k}(x) \left(\sum_{x_i > x} c_i\, f_{3k}(x_i) \right) + \sum_{k=1}^{M_2} p_{2k}\, f_{3k}(x) \left(\sum_{x_i < x} c_i\, f_{2k}(x_i) \right). \quad 57.$$

For multidimensional kernels written in tensor-product form, similar relations hold.

The simplest way to take advantage of this result is to precompute the sums for each box (that is, the sums over x_i in Equation 57). These sums can then be used to evaluate the representation at any point without having to recompute any sums over all the data points. An evaluation of the representation only requires one evaluation of a sum similar to Equation 56. Evaluation of the representation by use of this method can often be done with similar speed, or faster, than by use of analytic fits to the same data (87), no matter how many data points were used in the construction of the representation.

A careful analysis of this algorithm (12) shows that for a D-dimensional $N \times N \times \cdots \times N$ grid, a simple sum over all the ab initio data points requires approximately DN^D evaluations of the function $q(x, x')$, whereas the fast algorithm requires only about $(M_1 + M_2)^D$ evaluations. Since for many of the kernels $M_1 + M_2$ is a fairly small number (often 2, 3, 4 or 5), this can be a substantial speedup. For example, without use of the fast algorithm, interpolation on a large $20 \times 20 \times 20$ grid is about 64 times slower than interpolation on a small $5 \times 5 \times 5$ grid. When the fast algorithm is used (assuming a kernel with $M = 3$), both the small and large interpolations should be about five times faster than the smaller interpolation, and over 300 times faster than the larger one.

In order to demonstrate that this high speed can actually be achieved, independent of the number ab initio points, data was synthesized from a recent conventional fit to the $N(^2D) + H_2$ surface (87). The analytic fit was then used to construct a number of different RKHS representations of that surface with use of increasing numbers of grid points (12). As a test case, the analytic input surface allowed for direct observation of the interpolation error because there was a finite amount of information.

Figure 1 shows that the time required for evaluations of these surfaces is indeed independent of the number of synthesized ab initio points used. It is also significantly faster than the full sum over all the data points, whose cost grows quickly as the size of the grid increases. Not only is the $16 \times 16 \times 16$ point surface about 100 times faster with use of the fast algorithm, it also is about twice as fast as the original analytic surface it replaces. The root-mean-square difference between these two surfaces is only 1.32 kJ/mol, which demonstrates that the RKHS

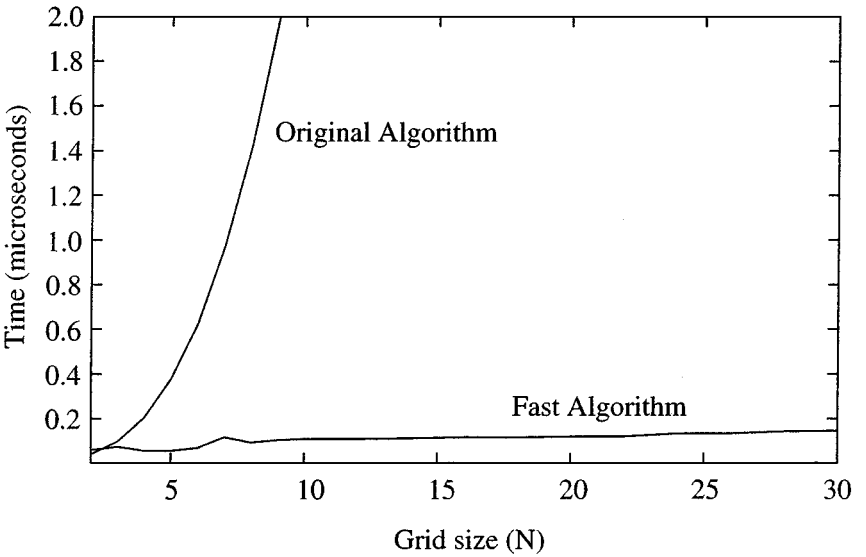

Figure 1 Time in microseconds for a single evaluation of the interpolated $N(^2) + H_2$ potential energy surface (PES) with and without the fast algorithm. N, the number of points per dimension; N^3, the total number of ab initio points.

method can quickly, efficiently, and accurately reconstruct a function from a finite number of evaluations. In a final example, the surfaces described in Ho et al (14) use this algorithm and thus reduce the evaluation time by a factor of 17 (from 7.7 ms to 128 μs on SGI Indigo2 R4400/200), which is significant in the dynamics calculations.

FAST-GRIDDED INTERPOLATION ON ARBITRARILY SHAPED REGIONS

The RKHS interpolation method has been introduced above in its general form, in which there are no restrictions on the locations of the points to be interpolated. The locations of ab initio points can be strategically placed in order to maximize the accuracy at, or near, important regions of the surface. The ability to do this is important when individual points are costly to obtain and only a relatively small number of calculations can be made.

The fast algorithm was introduced in the previous section and showed that there are significant advantages to the use of that points are arranged in a *D*-dimensional grid. The fast algorithm allows surfaces based on thousands of ab initio points to be evaluated efficiently, but it requires that the points be arranged in a *D*-dimensional grid. However, restriction to a *D*-dimensional grid can be inconvenient when

constructing representations of PESs. Often, an unacceptable fraction of the calculations required are at nonphysical, or at unimportant, geometries. In general, only a certain subset of the full configuration space is energetically accessible by means of dynamics studies, and ideally, ab initio calculations would be primarily done in that region, with sparser sampling done elsewhere. This section describes how the fast algorithm can still be used with this sort of data distribution. In fact, the surface obtained is identical to the results one would get in the general case of scattered points.

Three-atom reactive surfaces provide an excellent example of how this development can be helpful. In order to obtain correct long-range behavior for the entrance and exit channels, it is desirable to have a good number of points along both channels. But in most coordinate systems with a regular grid, this also implies the presence of a large number of points in the region where all three atoms are separated by large distances. Similarly, the grid also usually contains some points where two nuclei are extremely close to each other, unless the coordinate system is especially chosen to avoid this problem. Even if these points do not cause problems for the ab initio calculations, their extremely high energies can distort the interpolated PES. Lastly, the computer time that would have been spent on these unimportant regions of the surface can instead be used to improve the accuracy of the calculations in the dynamically important region.

As long as the kernel has the tensor-product form (Equation 22), it is possible to relax the full D-dimensional grid requirement, and this can alleviate many of the concerns introduced in the previous paragraph. First, if we have a solution to a particular interpolation problem with M arbitrarily placed points (Equation 7), then we can add new terms corresponding to points with zero coefficients and obtain the following solution:

$$f^{\dagger}(\mathbf{x}) = \sum_{i=1}^{M+M'} c'_i Q(\mathbf{x}_i, \mathbf{x}), \quad c'_i = c_i \quad \text{if } i \leq M, \quad \text{otherwise } c'_i = 0. \qquad 58.$$

This extension allows several practical insights. First, if we solve an interpolation problem in which the points are arranged in a subset of the full D-dimensional grid, we can treat it as a full grid simply by setting the coefficients of the uncalculated points to zero, which then allows the fast algorithm referred to above to be used. Since we just added terms with zero value to the function, the result is exactly the same function. The interpretation is that the zero value for the coefficient indicates that no information is available at that location, and that the value there should be interpolated based on the other points and the asymptotic properties of the kernel in the normal way. In addition, the coefficient matrix is now sparse, so the storage overhead is only proportional to the number of calculated points, and not to the size of the entire grid.

Second, since the solution to the interpolation problem is unique once a particular RKHS has been specified, we know that a set of coefficients that interpolates

the M points and has zero coefficients for the other M' points is the unique solution we are seeking. This can be done, for example, by solving the problem of scattering, then transfering the coefficients to the grid that contains it, and adding the zeros for the uncalculated points. However, because of the $O(N^3)$ scaling of matrix inversion, this may not be feasible for some very large data sets. In many common cases, this solution can be obtained without having to solve the M point problem with arbitararily placed points.

For example, if the M is larger than M', it is computationally advantageous first to solve the gridded problem with the use of arbitrary function values for the ab initio points that were not calculated. The values used do not change the final answer, so a simple local interpolation or an arbitrary constant will work. Better guesses can improve the numerical stability of the following process, but they do not change the answer for problems that do not suffer from any numerical instability. Let $g(\mathbf{x})$ be the solution found by doing the gridded interpolation using the arbitrary function values. Now, any solution can be written in terms of the cardinal functions:

$$f^{\dagger}(\mathbf{x}) = \sum_{i=1}^{M+M'} f_i \sum_{j=1}^{M+M'} [\mathbf{Q}]_{ij}^{-1} Q(\mathbf{x}_j, \mathbf{x}). \tag{59.}$$

The function $g(\mathbf{x})$ will agree with $f^{\dagger}(\mathbf{x})$ at the known points, so the difference is

$$g(\mathbf{x}) - f^{\dagger}(\mathbf{x}) = \sum_{i=M+1}^{M+M'} \delta_i \sum_{j=1}^{M+M'} [\mathbf{Q}]_{ij}^{-1} Q(\mathbf{x}_j, \mathbf{x}) \tag{60.}$$

for some unknown values δ_i. A comparison of this with Equation 7 shows that the difference in coefficients is

$$c_i - c_i^{\dagger} = \sum_{i=M+1}^{M+M'} \delta_i [\mathbf{Q}]_{ij}^{-1}, \tag{61.}$$

where $[\mathbf{Q}]_{ij}^{-1}$ is a $M' \times M'$ submatrix of the full $(M + M') \times (M + M')$ matrix $[\mathbf{Q}]^{-1}$. But we know c_i, and we know $c_i^{\dagger}$ is zero for the M' uncalculated points. Inversion of Equation 61 gives the δ_i values and hence the unknown values for $c_i^{\dagger}$. This solution interpolates the specified points and has zero coefficients at the uncalculated points, and hence, it must be the correct solution (Equation 58), because of the uniqueness of the RKHS solution.

This method allows the scattered-M-point problem to be solved with the effort expected for a M'-point problem. If the set of missing points has additional structure, the structure can often be exploited to reduce the complexity of the problem even further.

As an example, consider the 3-D $O(^1D) + H_2$ surface (14). Of the 1280 ab initio points used to generate that surface, only 560 are less than 50 mH (1.36 eV) above the bottom of the entrance channel. This corresponds to the classically

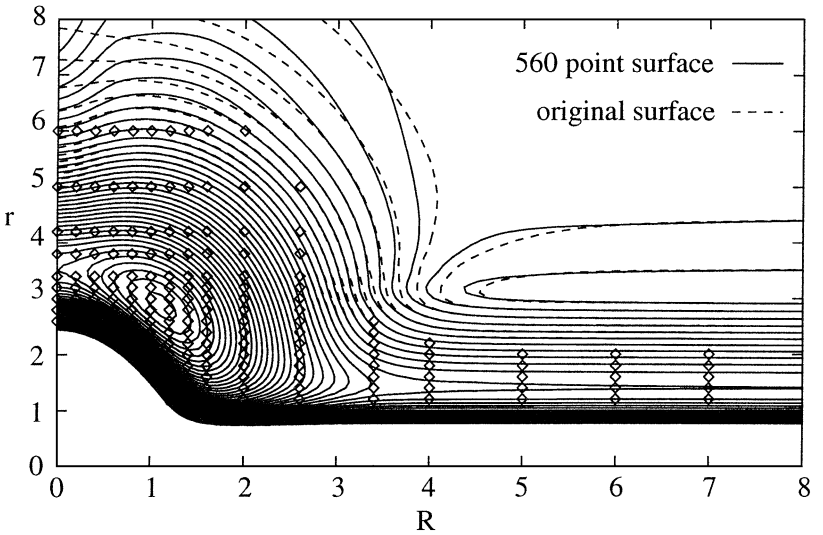

Figure 2 The contour plot comparing the original $O(^1D) + H_2$ surface based on 1280 ab initio points with a surface based only on the 560 points that are less than 50 mH above the entrance channel. The surfaces are identical in the region of the surface accessible at the highest scattering energies considered and agree qualitatively elsewhere. (*Contours*) At 10 mH intervals. The positions of the 169 C_{2v} points that are below the 50 mH cutoff are also shown. *r*, the H–H distance (in bohr); *R*, distance from the O atom to the H_2 midpoint.

accessible portions of the surface sampled by trajectories at approximately 26 kcal/mol. The highest energies considered in previous dynamical studies of this surface are more than a factor of two lower than that (14, 15).

Figure 2 shows how the points are distributed for C_{2v} geometries. Because this particular surface has a deep well (corresponding to the H_2O minimum), this example is closer to a worst-case scenario than to a typical one. A reaction with a narrower classically accessible reaction tube will require even fewer points. Figure 2 shows that the surface constructed from only 560 points is almost indistinguishable from the full 1280-point surface in the dynamically important region. Because of the many-body expansion and correct asymptotic form, it is also still quite accurate globally. The locations used here are simply the locations used in the initial construction; no attempt has been made to find a smaller subset that produces a surface with the same accuracy. This ability to deal with points placed within the dynamically important region makes it possible to construct, with only a few hundred ab initio calculations, global triatomic PESs that are chemically accurate (error <1 kcal/mol).

This same surface was very recently used to test the feasibility of using Shepard interpolation for this system (53). Along with the methods introduced in this

section, both methods can deal with data restricted to the dynamically important region. For Shepard interpolation, alternative point placement strategies were investigated because the trajectory sampling method used previously did not converge to an accurate surface quickly enough. It is interesting to note that some of the most accurate results were obtained simply by choosing random points in the dynamically important region, although the accuracy of the surfaces was not reported. Only the total cross section and average vibrational and rotational quantum numbers were monitored for convergence. Unfortunately, these observables are not particularly sensitive to PESs, and qualitatively different PESs can give relatively similar values (14). The Shepard results show that approximately 100 configurations (1000 pieces of data) are required to achieve convergence of these observables.

Incorportation of gradients and Hessians into RKHS potentials is straightforward because of the generalized spline nature of the kernels; however, this incorporation has not been performed in the past because analytic gradients and Hessians are not yet available in the package used for the calculations (14). With their inclusion, it is not unreasonable to expect that accurate triatomic potentials based on 50 or fewer calculations will become feasible.

REPRESENTATIVE SURFACES

To demonstrate some of the points made in the previous sections more concretely, we consider three examples as typical applications of the RKHS method to the construction of ab initio surfaces. The RKHS method has been used to construct a wide variety of different kinds of PESs. Previously published examples include a He–He potential, a 2-D potential surface for He–CO, and a 3-D surface for H_3^+ (11); global surfaces for the $1A'$ and $1A''$ states of $O(^1D) + H_2$ (14, 15) and $N(^2D) + H_2$ (16, 78, 79); and the lowest quartet state of Na_3 (76). The examples here focus on two cases of van der Waals surfaces and on a reactive surface.

The first two examples are 2-D PESs for the He–CO and Ar−OH($A\,^2\Sigma^+$) van der Waals complexes. Both these complexes have recently been extensively studied theoretically and experimentally (46–48, 88–93b). The topographies of the He–CO and Ar–OH are quite different in that the former is characterized by a global minimum at a skew geometry, whereas the latter has local minima at the collinear configurations Ar–O–H and Ar–H–O. The region around the global minimum of the He–CO interaction is flat, with a variation of $\sim$1 cm^{-1} over a 90° range starting from the T-shaped configuration to the linear He–C–O configuration. On the other hand, the two minima of the Ar–OH interaction for the $A\,^2\Sigma^+$ state are extremely deep, $\sim$1100 and 1000 cm^{-1}, respectively. In the last example, the methods introduced in the two previous sections are explored by using data from a previously published global surface for the reaction $O(^1D) + H_2 \rightarrow OH + H$ (14). These three examples illustrate many features of the RKHS interpolation method for multidimensional PES constructions using ab initio data.

RKHS surfaces depend on two pieces of input: the ab initio data, and the structure of interpolation space specified by the choice of reproducing kernel. In the case of van der Waals surfaces, the number of data points is typically small and the PES is quite smooth, so the details of the construction of the reproducing kernel are more important. In the reactive case, the number of data points often is significantly larger and less information is known about specific asymptotic forms, so efficient handling of the ab initio data and efficient sampling of the configuration space become the important issues, and the particular choice of kernel is less important. The flexibility of the RKHS method allows the handling of both kinds of problems without making significant changes in methodology.

The Two-Dimensional He–CO Interaction

The input ab initio data are 57 MP4 (fourth-order Moller-Plesset perturbation theory) calculations of Tao et al (46) on a regular grid, except one point, which is indicated in Figure 3. The He–CO PES $V(R, \theta)$ is considered to be a function of the Jacobi coordinates R and θ with the CO bond length fixed at $r = 1.128$ Å. To construct the regularized PES function $V_\alpha^\dagger(R, \theta)$, we introduce the new variables $x = R$ and $y = (1 + \cos\theta)/2$, so that $0 \le x < \infty$ and $0 \le y \le 1$, and adopt the 2-D reproducing kernel

$$Q_{n_1,m_1;n_2}(x, y, x', y') = q^{\mathrm{RP}}_{n_1,m_1}(x, x')q^{\mathrm{TS}}_{n_2}(y, y'), \qquad 62.$$

based on the RP and TS reproducing kernels described earlier. The 2-D contour plot in Figure 3 shows the PES function $V_\alpha^\dagger(R, \theta)$ based on the reproducing kernel $Q_{3,5;7}(x, y, x', y')$. Here, the regularization parameter α has been calculated according to the machine-roundoff error, as described previously. The high order of smoothness $n_2 = 7$ in the θ-direction compensates for the sparseness of the sampling of the surface. Lower values of n_2 produce surfaces that are slightly less smooth in the angular direction, and the relative error bound $\Delta_{R,\theta}(\alpha)$ correctly predicts the need for either more ab initio points or stronger smoothness constraints in this direction.

At the large distances, the PES $V_\alpha^\dagger(R, \theta)$ behaves as

$$-\left\{\frac{C_6(\theta)}{R^6} + \frac{C_7(\theta)}{R^7} + \frac{C_8(\theta)}{R^8}\right\} \qquad 63.$$

because of the use of the integers $n_1 = 3$ and $m_1 = 5$ for the RP reproducing kernel.

The Two-Dimensional Ar–OH ($A\,^2\Sigma^+$) Interaction

The input ab initio data are 87 CEPA (the coupled electron pair approximation) calculations of Esposti & Werner (94) on five evenly spaced angles in the θ-direction and on otherwise randomly spaced distances in the R-direction (see Figure 4). Here, the OH-bond is fixed at $r = 1.95$ bohr. The presence of two deep minima

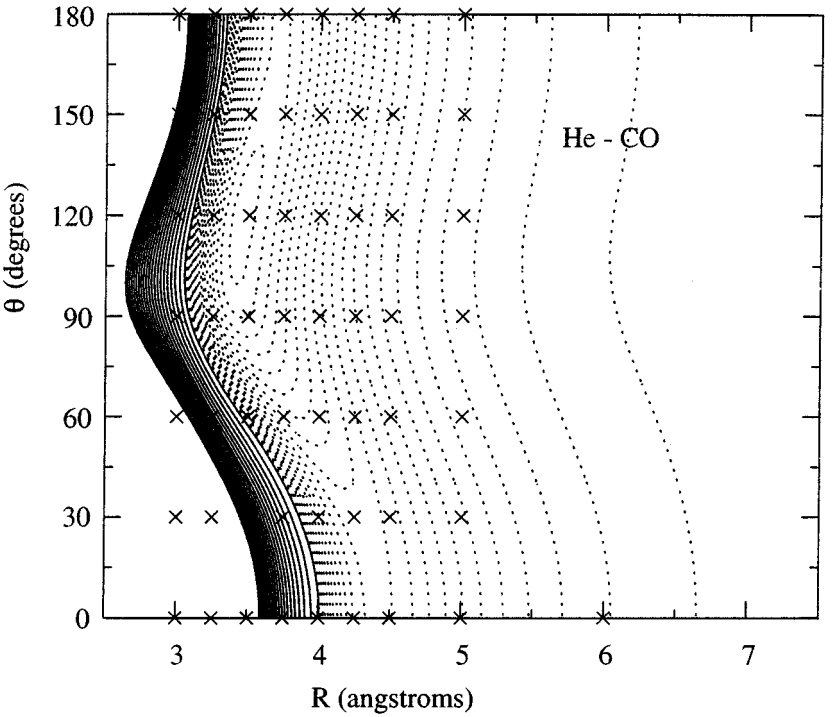

Figure 3 The contour plot of the reproducing Kernal Hilbert space (RKHS) potential energy surface (PES) for He–CO based on 57 fourth-order Moller-Plesset perturbation (MP4) ab initio data points of Tao et al (46). The RKHS PES is constructed using a two-dimensional tensor product of the one-dimensional reciprocal power (RP) and Taylor spline (TS) reproducing kernels as specified in Equation 62, with the parameters $n_1 = 3$, $m_1 = 5$, and $n_2 = 7$. (*Dotted contours*) Drawn in increments of 1.0 cm^{-1}, starting from a negative value -25 cm^{-1}, up to zero; (*solid contours*) drawn in increments of 5.0 cm^{-1} from the zero up to 25 cm^{-1}. $\times$, Indicates where the ab initio calculations were made.

at collinear geometries corresponding to isomeric OH–Ar and Ar–OH structures requires the sampling of more ab initio data points around the minima in the *R*-direction. To construct the 2-D Ar–OH($A\ ^2\Sigma^+$) potential, the same 2-D reproducing kernel is adopted, along with the simple form of regularization parameter based on the machine-roundoff error, as was done in the preceding He–CO interaction case. To describe these deep wells, especially the one at the collinear Ar–O–H configuration, we have chosen $n_1 = 4$ and $m_1 = 5$ for the distance RP reproducing kernel, in conjunction with $n_2 = 2$ for the angular TS reproducing kernel. A comparison of Figures 4 and 5 shows that the error bound indicates that much of the remaining uncertainty in the resultant PES function $V_\alpha^\dagger(R, \theta)$ exists in between the five evenly spaced angular data points because of the low order of

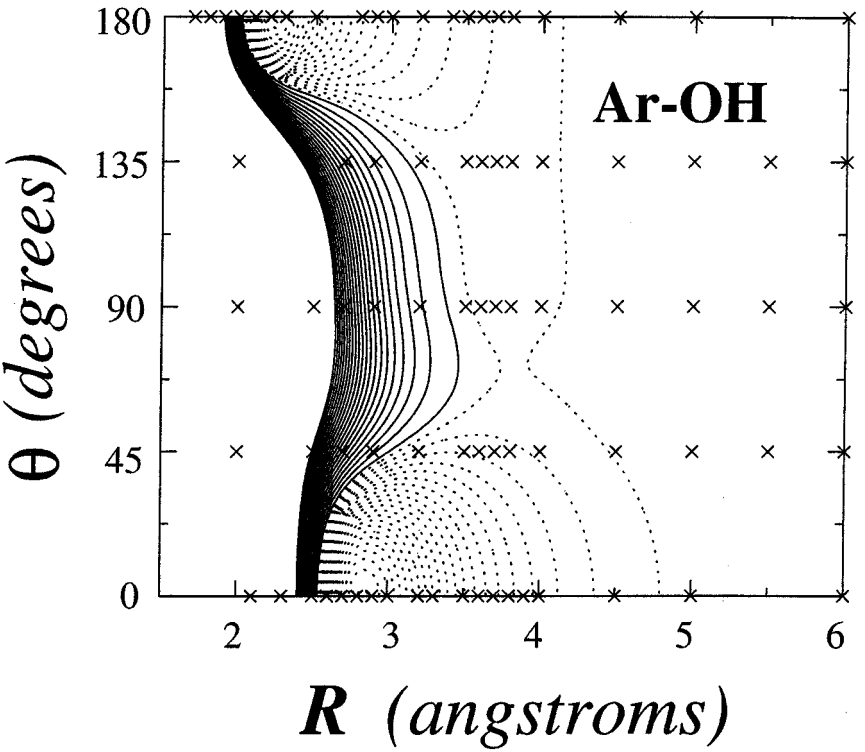

Figure 4 The contour plot of the reproducing Kernel Hilbert space (RKHS) potential energy surface (PES) for Ar–OH ($A\ ^2\Sigma^+$) based on 87 CEPA ab initio data points of Esposti & Werner (94). The RKHS PES is constructed using a two-dimensional tensor product of the one-dimensional reciprocal power (RP) and Taylor spline (TS) reproducing kernels as specified in Equation 62, with the parameters $n_1 = 4$, $m_1 = 5$, and $n_2 = 2$. (*Dotted contours*) Drawn in increments of 50.0 cm^{-1} from the starting value -1100 cm^{-1} up to zero; (*solid contours*) drawn in increments of 100.0 cm^{-1} from zero up to 1000 cm^{-1}. $\times$, Indicates where the ab initio calculations were made.

smoothness $n_2 = 2$ in the TS reproducing kernel, whereas the uncertainty in the R-direction along the cuts at various data angles is very small because of the relatively high order of smoothness $n_1 = 4$ in the RP reproducing kernel and the higher density of points along that dimension. Again, a higher value of n_2 produces a slightly smoother surface, showing the usefulness of the error bound in the choice of the appropriate reproducing kernel for a particular problem. The (relative) error bound clearly becomes increasingly small toward larger R distances, as a result of a reciprocal weight on the order of $m_1 = 5$.

The two examples above demonstrate that the RKHS interpolation method can render accurate and globally smooth multidimensional PESs based on relatively

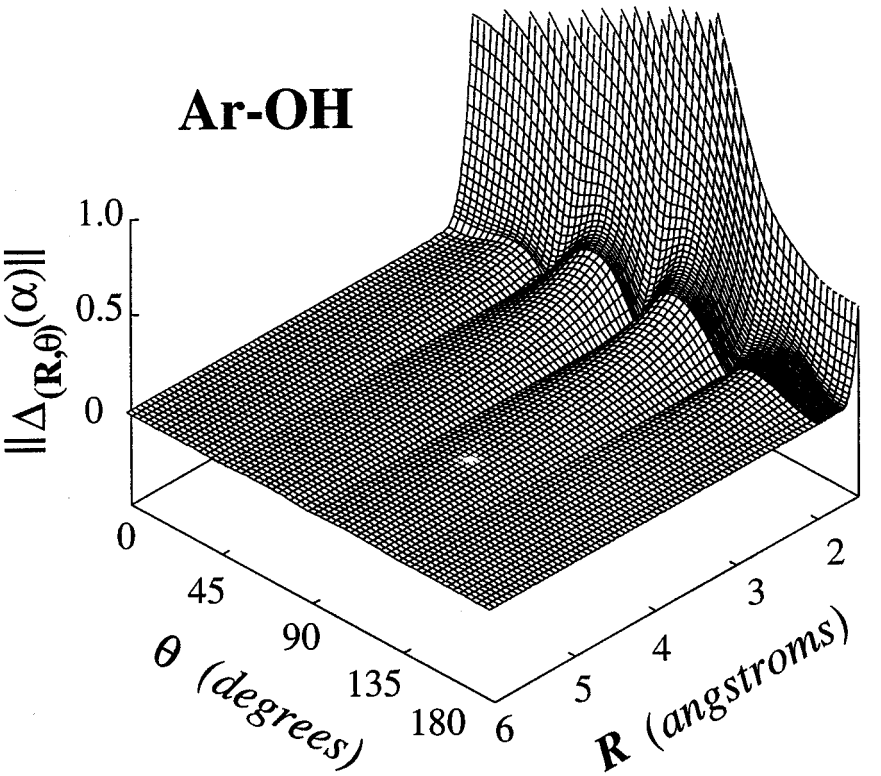

Figure 5 The relative error bound $\|\Delta_{(R,\theta)}(\alpha)\|(\times 10^3)$, corresponding to the reproducing Kernel Hilbert space (RKHS) potential energy surface (PES) for Ar–OH($A\ ^2\Sigma^+$) depicted in Figure 4, is shown as a function of the Jacobi coordinates R and θ. The ups and downs inbetween the interpolated ab initio data points reveal the extent of relative uncertainties of the corresponding RKHS PES.

small sets of ab initio data. They also show that the correct asymptotic form of the intermolecular interaction can be incorporated into the construction of the underlying PES in a straightforward fashion.

The Three-Dimensional $O(^1D) + H_2$ Reaction

The final example shows how to apply the fast algorithm, formulated within the RKHS method (see above), to facilitate the evaluation of high-dimension PESs constructed with relatively large numbers of ab initio data points. For an illustration, consider the specific example of a 3-D PES for the reactive system $O(^1D) + H_2$ (14). This particular surface was the first illustration of the RKHS method for the representation of PESs for reactive systems, and the PES has been well studied

dynamically (14, 15, 95, 96). Some observations and a discussion follow about improvements to the methods used to construct that particular surface, and which have also been used in more recent constructions of surfaces (77).

For a reactive system, it is useful to write the PES as a many-body expansion (7) where the energy is expressed in terms of the energies of smaller fragments (14, 15):

$$V_{HHO}(R_1, R_2, R_3) = V^{(1)} + V_{OH}^{(2)}(R_1) + V_{OH}^{(2)}(R_2) + V_{HH}^{(2)}(R_3) + V_{HHO}^{(3)}(R_1, R_2, R_3), \quad 64.$$

which guarantees that the energies of the reactants and products will be accurate. However, in reactive systems, the physical basis of this expansion is less sound than it is for van der Waals systems, because it implies that the ground state of water contains an H–H–bonding interaction. Although this does not adversely impact the accuracy of the final potential, it does suggest that a more careful choice of lower-dimensional terms (for example, something similar in conception to a DIM surface) might be useful to reduce the number of points needed to represent the three-body interaction. For larger systems, such considerations are even more important.

The two-body terms are 1-D functions, so a relatively small number of points can pin down their behavior precisely. For the H–H and O–H terms, respectively, 48 and 52 points were used, and the data was interpolated using $q_{2.0}^{\mathrm{RP}}$. The three-body term was interpolated on a regular 3-D grid in a coordinate system based on Jacobi coordinates [$x = \exp(-0.5R), y = \exp(-0.3r), z = 2\sin\theta - 1$]. Although Jacobi coordinates are convenient for atom-diatom complexes and from a scattering point of view, the fact that two nuclei overlap along a line running diagonally ($R = r$) through the $\theta = 0$ slice complicates the construction process. Coordinate systems that treat the internuclear distances on a more equal footing, like the perimetric coordinate system ($s_1 = R_2 + R_3 - R_1$, $s_2 = R_1 + R_3 - R_2$, $s_3 = R_1 + R_2 - R_3$), may simplify the construction process and reduce the number of points needed to achieve accurate results. The kernels used to interpolate the three-body term were q_2^{TS} for x and y, and the following kernel, based on normalized Legendre polynomials, was used for z (see Equation 53):

$$K(z, z') = \sum_{k=0}^{n} p_k(z)\, p_k(z'). \quad 65.$$

Numerous theoretical studies of this surface have appeared since it was introduced. For the first time, both classical and QM calculations (14, 96) are in qualitative agreement, and sometimes, in near-quantitative agreement, with experimental results (97, 98). Efforts to explain the remaining disagreements due to the influence of excited states and the conical intersection present in this system (15, 99, 100) continue.

CONCLUSIONS

Over the past few decades, single–point electronic structure calculations have had a tremendous impact on the study of chemical systems. Similar progress in chemical dynamics has been limited both by the larger number of calculations necessary for such studies and also by the difficulties in converting high-quality ab initio data sets into surfaces that preserve the quality of the data. With the continued steady improvement of electronic structure calculations and of computational hardware, the treatment of larger and more complex systems will soon be feasible. Recent and anticipated future advances concerning the methodology for the construction of PES representations will allow these calculations to be utilized without having to make unnecessary approximations.

The construction of representations of the $O + H_2$ and $N + H_2$ PESs using the RKHS tools has shown that the method can generate accurate and efficient triatomic PESs without making ad hoc assumptions. In addition, a comparison of the dynamics on those surfaces with recent experimental data has demonstrated that the RKHS surfaces are more accurate than were previously available surfaces. Studies of the dynamics in both the ground and excited states of both systems have demonstrated the importance of excited states and surface crossings in the dynamics of chemical systems. Work to explicitly include couplings between surfaces within a unified framework is in progress. Although continued refinements of the method are still possible, even for triatomics, the means for construction of high-accuracy triatomic surfaces already exist, and a software package that implements the RKHS method will be made available. The technique has flexibility (for example, in the choice of reproducing kernel), and it can be made systematic for new user applications.

The RKHS method has also been applied to a number of van der Waals systems. The issues involved in the construction of such surfaces are often different from those involved in the construction of reactive surfaces, and the capacity in the RKHS method to construct both kinds of surfaces demonstrates the flexibility of the method.

For van der Waals systems, the important advantages in the RKHS method are the ability to deal with scattered data within a uniform framework that has the ability to impose asymptotic forms and symmetry constraints in a consistent manner. Recent work has compared the results to high-accuracy spectroscopic studies of the quartet Na_3 system (76) with considerable success.

In reactive systems, the fast algorithm allows the efficient use of as many ab initio calculations as are required to properly represent the system while allowing calculations to be concentrated in dynamically important regions, and it gives the RKHS method the capability to generate reaction path surfaces without the use of curvilinear coordinates. In addition, the error bound provides a consistent method for assessment of the quality of surfaces and offers information regarding where more calculations are necessary.

ACKNOWLEDGMENTS

We are pleased to acknowledge a fruitful collaboration with Larry Harding and George Schatz on various aspects of RKHS development and implementation. This work was supported by the US Department of Energy.

LITERATURE CITED

1. Yamaguchi Y, Osamura Y, Goddard JD, Schaefer HF III. 1994. *A New Dimension to Quantum Chemistry*. New York-Oxford: Oxford Univ. Press
2. Hehre WJ, Radom L, Schleyer P, Pople JA. 1996. *Ab Initio Molecular Orbital Theory*. New York: Wiley
3. Head-Gordon M. 1996. *J. Phys. Chem.* 100:13213–25
4. Kohn W, Becke AD, Parr RG. 1996. *J. Phys. Chem.* 100:12974–80
5. Dunning TH Jr., ed. 1990. *Advances in Molecular Electronic Structure Theory*, Vol. 1. London: Jai
6. Jeziorski B, Moszynski R, Szalewicz K. 1994. *Chem. Rev.* 94:1887–930
7. Murrell JN, Carter S, Farantos SC, Huxley P, Varandas AJC. 1984. *Molecular Potential Energy Functions*. New York: Wiley
8. Truhlar DG, Steckler R, Gordon MS. 1987. *Chem. Rev.* 87:217–36
9. Schatz GC. 1989. *Rev. Mod. Phys.* 61: 669–88
10. Ischtwan J, Collins MA. 1994. *J. Chem. Phys.* 100:8080–88

10a. Collins MA. 1996. *Adv. Chem. Phys.* 93: 389–453

11. Ho TS, Rabitz H. 1996. *J. Chem. Phys.* 104:2584–97
12. Hollebeek T, Ho TS, Rabitz H. 1997. *J. Chem. Phys.* 106:7223–27
13. Ho TS, Rabitz H. 1998. In *CCP6, Fashioning a Model: Optimization Methods in Chemical Physics*, ed. A Ernesti, JM Hutson, NJ Wright, pp. 28–34
14. Ho TS, Hollebeek T, Rabitz H, Harding LB, Schatz GC. 1996. *J. Chem. Phys.* 105: 10472–86
15. Schatz GC, Papaioannou A, Pederson LA, Harding LB, Hollebeek T, et al. 1997. *J. Chem. Phys.* 107:2340–50
16. Alagia M, Balucani N, Cartechini L, Casavecchia P, Volpi GG, et al. 1999. *J. Chem. Phys.* In press
17. Helgaker T, Uggerud E, Jensen HJA. 1990. *Chem. Phys. Lett.* 173:145–50
18. Chen W, Hase WL, Schlegel HB. 1994. *Chem. Phys. Lett.* 228:436–42
19. Steckler R, Thurman GM, Watts JD, Bartlett RJ. 1997. *J. Chem. Phys.* 106: 3926–33
20. Varandas AJC, Abreu PE. 1998. *Chem. Phys. Lett.* 293:261–69
21. Chuang Y-Y, Truhlar DG. 1997. *J. Phys. Chem.* 101:3808–14
22. Corchado JC, Espinosa-Garcia J, Roberto-Neto O, Chuang Y-Y, Truhlar DG. 1998. *J. Phys. Chem. A* 102:4899–910
23. Jordan JT, Thompson KC, Collins MA. 1995. *J. Chem. Phys.* 102:5647–57

23a. Jordan JT, Thompson KC, Collins MA. 1995. *J. Chem. Phys.* 103:9669–75

23b. Jordan JT, Collins MA. 1996. *J. Chem. Phys.* 104:4600–10

24. Thompson KC, Collins MA. 1997. *J. Chem. Soc. Faraday Trans.* 93:871–78

24a. Thompson KC, Jordan JT, Collins MA. 1998. *J. Chem. Phys.* 108:564–78

24b. Thompson KC, Jordan JT, Collins MA. 1998. *J. Chem. Phys.* 108:8302–16

25. Ishida T, Schatz GC. 1997. *J. Chem. Phys.* 107:3558–68

26. Takata T, Taketsugu T, Hirao K, Gordon MS. 1998. *J. Chem. Phys.* 109:4281–89
27. Siegbahn P, Liu B. 1978. *J. Chem. Phys.* 68:2457–65
28. Truhlar DG, Horowitz J. 1978. *J. Chem. Phys.* 68:2466–76

28a. Truhlar DG, Horowitz J. 1979. *J. Chem. Phys.* 71:1514

29. Boothroyd AI, Keogh WJ, Martin PG, Peterson MR. 1991. *J. Chem. Phys.* 95: 4343–59
30. Boothroyd AI, Keogh WJ, Martin PG, Peterson MR. 1996. *J. Chem. Phys.* 104: 7139–52
31. Beck C, Keller HM, Grebenschikov SY, Schinke R, Farantos SC, Yamashita K, Morokuma K. 1997. *J. Chem. Phys.* 107: 9818–34
32. Gonzalez M, Hijazo J, Novoa JJ, Sayos R. 1998. *J. Chem. Phys.* 108:3168–77
33. Aguado A, Paniagua M. 1992. *J. Chem. Phys.* 96:1265–75

33a. Aguado A, Tablero C, Paniagua M. 1998. *Comp. Phys. Commun.* 108:259–66

34. Aguado A, Paniagua M, Lara M, Roncero O. 1997. *J. Chem. Phys.* 107:10085–95
35. Varandas AJC. 1996. *J. Chem. Phys.* 105: 3524–31

35a. Varandas AJC. 1997. *J. Chem. Phys.* 107: 5987

36. Varandas AJC. 1997. *J. Chem. Phys.* 107: 867–78
37. Varandas AJC, Voronin AI, Caridade PJ. 1998. *J. Chem. Phys.* 108:7623–30
38. Varandas AJC, Voronin AI. 1995. *Mol Phys.* 85:497–526
39. Varandas AJC, Yu HG. 1997. *Mol. Phys.* 91:301–18
40. Kuntz PJ, Niefer BI, Sloan JJ. 1988. *J. Chem. Phys.* 88:3629–37

40a. Kuntz PJ, Niefer BI, Sloan JJ. 1991. *Chem. Phys.* 151:77–93

41. Kinghorn DB, Adamowicz L. 1997. *J. Chem. Phys.* 106:8760–8
42. Hutson JM. 1988. *J. Chem. Phys.* 89: 4550–57
43. Moszynski R, Wormer PES, van der Avoird A. 1995. *J. Chem. Phys.* 102: 8385–97
44. Stark K, Werner HJ. 1996. *J. Chem. Phys.* 104:6515–30
45. Topaler MS, Truhlar DG, Chang XY, Piecuch P, Polanyi JC. 1998. *J. Chem. Phys.* 108:5349–77
46. Tao FM, Drucker S, Cohen RC, Klemperer W. 1994. *J. Chem. Phys.* 101:8680–86
47. Heijmen TG, Moszynski R, Wormer PES, ver der Avoird A. 1997. *J. Chem. Phys.* 107:9921–28
48. Marshall PJ, Szczesniak MM, Sadlej J, ChaIasinki G, ter Horst MA, Jameson CJ. 1996. *J. Chem. Phys.* 104:6569–76
49. ter Horst MA, Schatz GC, Harding LB. 1996. *J. Chem. Phys.* 105:558–71
50. Alagia M, Balzecani N, Casavecchia P, Stranges D, Volpi GG, et al. 1996. *Chem. Phys.* 207:389–409
51. Wu YSM, Kuppermann A, Anderson JB. Submitted for publication
52. Diedrich DL, Anderson JB. 1992. *Science* 258:786–88

52a. Diedrich DL, Anderson JB. 1994. *J. Chem. Phys.* 100:8089–95

53. Ishida T, Schatz GC. 1998. *Chem. Phys. Lett.* 298:285–92
54. Schulz S, de Vivie-Riedle R. 1997. *Comput. Phys.* 11:647–59
55. Bettens RPA, Collins MA. 1998. *J. Chem. Phys.* 108:2424–33
56. Nguyen KA, Rossi I, Truhlar DG. 1995. *J. Chem. Phys.* 103:5522–30
57. Rhee YM, Lee TG, Park SC, Kim MS. 1997. *J. Chem. Phys.* 106:1003–12

57a. Rhee YM, Kim MS. 1998. *J. Chem. Phys.* 109:5363–71

58. Jäckle A, Meyer HD. 1996. *J. Chem. Phys.* 104:7974–84

58a. Jäckle A, Meyer HD. 1998. *J. Chem. Phys.* 109:3773–9

59. Hoffman DK, Frishman A, Kouri DJ. 1996. *Chem. Phys. Lett.* 262:393–99

59a. Frishman A, Hoffman DK, Kouri DJ. 1997. *J. Chem. Phys.* 107:804–11

60. Schaback R. 1997. In *Proceedings of Chamonix 1996*, ed. AL Mehaute, C Rabut, LL Schumaker, pp. 309–18. Nashville, TN: Vanderbilt Univ. Press
61. Aronszajn N. 1950. *Trans. Am. Math. Soc.* 68:337–404
62. Davis PJ. 1975. *Interpolation and Approximation*. New York: Dover
63. Hille E. 1972. *Rocky Mount. J. Math.* 2:321–68
64. Weinert H, ed. 1982. *Reproducing Kernel Hilbert Spaces: Applications in Statistical Signal Processing*. Stroudsburg, PA: Hutchinson Ross
65. Bergman S. 1946. *Am. J. Math.* 68:20–28
66. Mercer J. 1909. *Philos. Trans. R. Soc. London Ser. A* 209:415–46

66a. Mercer J. 1911. *Philos. Trans. R. Soc. London Ser. A* 211:111–98

67. Bergman S, Schiffer M. 1948. *Duke Math. J.* 15:535–66
68. Loéve M. 1948. In *Stochastic Processes and Brownian Motion*, ed. P Levy. Paris: Gauthier-Villars. Appendix (In French)
69. de Boor C, Lynch R. 1966. *J. Math. Mech.* 15:953–69
70. Mansfield LE. 1971. *SIAM J. Numer. Anal.* 8:115–26

70a. Mansfield LE. 1972. *J. Approx. Theory* 5:77–96

71. Nielson GM. 1974. *SIAM J. Numer. Anal.* 11:435–46
72. Duchon J. 1977. In *Constructive Theory of Functions of Several Variables*, ed. W Schempp, Z Keller, pp. 85–100. Berlin-Heidelberg: Springer-Verlag
73. Meinguet J. 1979. *J. Appl. Math. Phys.* 30:292–304
74. Adams RA. 1975. *Sobolev Spaces*. New York: Academic
75. Wahba G. 1990. *Spline Models for Observational Data*. Philadephia, PA: SIAM
76. Higgins J, Hollebeek T, Reho J, Ho TS, Lehmann KK, et al. Manuscript in preparation
77. Hollebeek T, Ho TS, Rabitz H, Harding LB. Manuscript in preparation
78. Schatz GC, Pederson PA, Ho TS, Hollebeek T, Rabitz H, et al. 1999. *J. Chem. Phys.* In press
79. Schatz GC, Pederson PA, Ho TS, Hollebeek T, Rabitz H, Harding LB. Manuscript in preparation
80. Hu XG, Ho TS, Rabitz H. 1998. *Chem. Phys. Lett.* 288:719–26
81. Hu XG, Ho TS, Rabitz H. 1998. *Comput. Phys. Commun.* 113:168–79
82. Bertero M, Mol CD, Pike ER. 1985. *Inverse Probl.* 1:301–30

82a. Bertero M, Mol CD, Pike ER. 1988. *Inverse Probl.* 4:573–94

83. Press WH, Teukolsky SA, Wettering WT, Flannery BP. 1992. *Numerical Recipes in Fortran*. Cambridge: Cambridge Univ. Press. 2nd ed.
84. Tikhonov AN, Arsenin V. 1977. *Solution of Ill-Posed Problems*. Washington, DC: Winston/Wiley
85. Abramoivitz M, Stegun I. 1972. *Handbook of Mathematical Functions*, Chap. 23, pp. 803–19. New York: Dover
86. Abramouwitz M, Stegun I. 1972. *Handbook of Mathematical Functions*, Chap. 22, pp. 771–802. New York: Dover
87. Kobayashi H, Takayanagi T, Yokoyama K, Sato T, Tsunashima S. 1995. *J. Chem. Soc. Faraday Trans.* 91:3771–77
88. Chuaqui CE, Le Roy RJ, McKeller ARW. 1994. *J. Chem. Phys.* 101:39–61
89. Chan MC, McKeller ARW. 1996. *J. Chem. Phys.* 105:7910–14
90. Bowman JM, Gazdy B, Schafer P, Heaven MC. *J. Phys. Chem.* 94:2226

90a. Schnupf U, Bowman JM, Heaven MC. 1992. *Chem. Phys. Lett.* 189:487–94

91. Fawzy WM, Heaven MC. 1988. *J. Chem. Phys.* 89:7030–33

91a. Fawzy WM, Heaven MC. 1990. *J. Chem. Phys.* 92:909–16

91b. Heaven MC. 1993. *J. Phys. Chem.* 97: 8567–77

92. Ho TS, Rabitz H, Choi SE, Lester MI. 1996. *J. Chem. Phys.* 104:1187–202

92a. Zhang DH, Light JC. 1995. *J. Chem. Phys.* 103:9713–20
92b. Wu Q, Zhang JZH. 1996. *Chem. Phys. Lett.* 252:195–200
93. Lester MI, Loomis RA, Giancarlo LC, Berry MT, Chakravarty C, Clary DC. 1993. *J. Chem. Phys.* 98:9320–34
93a. Lester MI, Randall RW, Giancarlo LC, Choi SE. 1993. *J. Chem. Phys.* 99:6211–14
93b. Choi SE, Lester MI, Jang HW, Light JC. 1995. *J. Chem. Phys.* 102:1981–93
94. Esposti AD, Werner HJ. 1990. *J. Chem. Phys.* 93:3351–66
95. Alexander AJ, Aoiz FJ, Bañares L, Brouard M, Herrero VJ, Simons JP. 1997. *Chem. Phys. Lett.* 278:313–24
96. Balint-Kurti GG, Gonzalez AI, Goldfield EM, Gray SK. 1998. *Faraday Discuss.* 110:169–83
97. Alagia M, Balucani N, Cartechini L, Casavecchia P, van Kleef EH, et al. 1998. *J. Chem. Phys.* 108:6698–708
98. Hsu YT, Wang JH, Liu KP. 1997. *J. Chem. Phys.* 107:2351–56
99. Yarkony DR. 1998. *Mol. Phys.* 93:971–83
100. Schatz GC, Pederson LA, Kuntz PJ. 1997. *Faraday Discuss.* 108:357–74